Gas and Vapor Sorption, Permeation, and Diffusion in Poly(tetrafluoroethylene-*co*-perfluoromethyl vinyl ether)

Rajeev S. Prabhakar,[†,⊥] Maria Grazia De Angelis,[‡] Giulio C. Sarti,[‡] Benny D. Freeman,*[,†] and Michael C. Coughlin[§]

Department of Chemical Engineering, University of Texas at Austin, 10100 Burnet Road, Bldg. 133, Austin, Texas 78758; Dipartimento di Ingegneria Chimica, Mineraria e delle Tecnologie Ambientali, Universita' di Bologna, Viale Risorgimento 2, 40136 Bologna, Italy; and DuPont Dow Elastomers L.L.C., Wilmington, Delaware 19809

Received March 14, 2005; Revised Manuscript Received May 17, 2005

ABSTRACT: Solubilities of N_2, CO_2, C1−C3 saturated hydrocarbons, C1−C3 saturated fluorocarbons, and normal- and cyclo-C5 and -C6 alkanes at 35 °C are reported in an amorphous, rubbery, random copolymer composed of 50.7 mol % tetrafluoroethylene and 49.3 mol % perfluoromethyl vinyl ether, TFE/PMVE49. Permeabilities of N_2, O_2, CO_2, and C1−C3 saturated hydrocarbons in this polymer at 35 °C are also presented. Solubilities of hydrocarbon vapors in this fluoropolymer are lower than those of their corresponding fluorocarbon analogues due to less favorable interactions of the fluorinated polymer with hydrocarbon vapors than with fluorocarbon penetrants. Polymer density was measured over a wide temperature and pressure range to estimate parameters for equation-of-state modeling of gas sorption. Modeling the sorption isotherms with the Sanchez−Lacombe equation-of-state model requires a reduction of approximately 10% in the cohesive energy density of the gas−polymer mixture from that predicted by the geometric mean mixing rule for all hydrocarbon penetrants other than CH_4. Sorption of CH_4 and fluorocarbon penetrants is well described with little or no variation in the geometric mean rule estimate of interaction energy. While linear correlations between the natural logarithm of hydrocarbon gas solubility and penetrant critical temperature in hydrocarbon polymers often have slope values of about 0.019 K^{-1} at 35 °C, this fluoropolymer has a much lower slope value, 0.011 K^{-1}. Hydrocarbon/nitrogen permeability selectivity is much lower in TFE/PMVE49 than in hydrocarbon-based rubbery polymers such as poly(dimethylsiloxane). This effect is, to a very large extent, a result of hydrocarbon solubility suppression in the fluoropolymer, due to less favorable hydrocarbon−fluorocarbon interactions.

Introduction

Gas separation polymer membranes often derive high permeability selectivities from differences in gas diffusion coefficients. Gas diffusivity values in polymers often vary over much wider ranges than gas solubility coefficients.[1] Moreover, gas diffusion coefficients and diffusivity selectivity values may be varied greatly by varying polymer structure. Therefore, structural modifications to alter gas diffusivity have traditionally been the focus of studies to prepare better gas separation membranes.[1,2] However, high diffusivity selectivity of polymer membranes can be significantly impaired by the action of gases and vapors that have high solubilities in the polymers.[3,4] These penetrants can plasticize polymer membranes and increase polymer chain mobility, which reduces the size-sieving ability (i.e., diffusivity selectivity) of the polymer.[5−8] As a result, several investigations have focused on the deleterious effect of high gas solubility on separation properties.[3,9−13]

Gas solubility in polymers is often correlated with measures of gas condensability such as normal boiling point temperature, T_b,[14,15] Lennard-Jones force constant, (ϵ/k),[16,17] and critical temperature, T_c.[14,18] Gas solubility in liquids also obeys similar correlations.[19] For example, on the basis of solubility data of over 15 gases (including permanent gases, noble gases, hydrocarbons, and others like H_2S, SO_2, and NH_3) in 15 different organic liquids (with solubility varying over 3 orders of magnitude), Korosy found that "the logarithm of solubility is nearly a linear function of the critical temperature of the gas and that the slope of these straight lines is about the same for all solvents".[19] Thus, solubility, S, can be expressed as follows:

$$\ln S = a + bT_c \tag{1}$$

where the intercept, a, and slope, b, are adjustable constants. Since this linear relationship was observed for gases as different as helium and sulfur dioxide, Korosy concluded that "gas solubility is governed to a first approximation by 'physical' forces, while 'chemical affinity' only modifies their action to a small extent and probably causes the deviation of certain points from the straight lines".[19] The use of this linear relationship in correlating gas solubility in polymers[17,20−23] has revealed similar b values to those observed in liquids[19] (cf. Tables 1 and 2).

Gee provided a simple theoretical framework for the observed correlation between gas solubility in rubbery polymers and gas condensability by considering gas solubility to be a hypothetical two-step process involving condensation of the gas to a liquidlike density followed by dilution of the gas in the polymer (i.e., mixing of gas molecules and polymer chains).[15] His correlation, in terms of the gas boiling point, modified using the Guldberg−Guye rule[18] relating boiling and critical tem-

† University of Texas at Austin.
‡ Universita' di Bologna.
§ DuPont Dow Elastomers L.L.C.
⊥ Current address: MEDAL L.P., Newport, DE 19804.
* Corresponding author: e-mail freeman@che.utexas.edu; Ph (512) 232-2803; Fax (512) 232-2807.

10.1021/ma050546b CCC: $30.25
Published on Web 07/13/2005

Table 1. Slope Values, *b*, of the Linear Relationship between ln *S* and T_c for Gas Solubility in Organic Liquids at 20 °C[19]

solvent	$b \times 10^3$ (K^{-1})	solvent	$b \times 10^3$ (K^{-1})
methyl alcohol	14	toluene	14
ethyl alcohol	15	xylene	13
amyl alcohol	16	cyclohexane	16
ethyl ether	14	cyclohexanol	13
acetone	17	tetrachloromethane	15
methyl acetate	16	chloroform	19
ethyl acetate	15	chlorobenzene	19
benzene	18		

Table 2. Slope Values, *b*, of the Linear Relationship between ln *S* and T_c for Gas Solubility in Polymers

classification	medium	$b \times 10^3$ (K^{-1})
rubbers	natural rubber[17]	18[a]
	amorphous polyethylene[17]	16[a]
	poly(butadiene)-hydrogenated[17]	17[a]
	poly(dimethylsiloxane)[20]	17[b]
glassy polymers	polysulfone[21]	17[c]
	poly(phenylene oxide)[22]	16[d]
	poly(ethylene terephthalate)[23]	19[e]

[a] 25 °C and 1 atm. [b] 35 °C. [c] 35 °C and 10 atm for all gases except *n*-C_4H_{10}, which is at infinite dilution. [d] 35 °C and infinite dilution. [e] 24−45 °C and infinite dilution.

peratures (i.e., $T_b = 0.6T_c$), is

$$\ln S = -(4.5 + \chi) + \left(\frac{0.6\Delta S_{vap}}{RT}\right)T_c \qquad (2)$$

where S is gas solubility in the polymer in units of cm^3 (STP)/(cm^3 polymer atm), χ is the Flory−Huggins interaction parameter, ΔS_{vap} is the entropy of vaporization of the penetrant gas at its normal boiling point and has a value of 20 cal/(mol K) according to Trouton's rule,[15,24] R is the universal gas constant (1.987 cal/(mol K)), and T is absolute temperature (K). Comparing eqs 1 and 2 provides a simple relation for the slope, b, when ln S is described as a linear function of T_c:

$$b \cong \frac{6}{T} \qquad (3)$$

This relation predicts a b value of 0.019 K^{-1} at 35 °C. Equation 3 is strictly valid for equilibrium matrices like liquids and rubbery polymers, but gas solubility in glassy polymers also often exhibits similar trends. In this regard, Table 2 displays the slope values for the least-squares best fit straight lines to solubility data for some glassy polymers.

Specific interactions between gas molecules and polymer chains can cause deviations in the gas solubility from the expected value based on the ln $S-T_c$ correlation. For example, significant deviations have been found for CO_2 solubility in many polymers.[14,25−27] The quadrupole moment of CO_2 enables specific interactions with polar groups on polymer chains.[26] Such effects can offer an additional degree of freedom in tailoring the separation characteristics of polymer membranes.[28]

Recently, fluorocarbon penetrants like CF_4, C_2F_6, and C_3F_8 have been discovered to exhibit much lower solubility in hydrocarbon polymers like poly(dimethylsiloxane) (PDMS) than expected on the basis of their critical temperature.[29] For example, the solubility of CF_4 in PDMS is 3 times lower than that expected from the ln $S-T_c$ relationship.[30] A description of the solubility behavior using the Sanchez−Lacombe equation-of-state model results in values for the binary interaction parameter for fluorocarbon gas−PDMS interactions that are ≈10% less than those for hydrocarbon gas−PDMS interactions, indicating relatively weak interactions between PDMS and fluorocarbon gases.[31] If the interactions between fluorocarbons and hydrocarbons are generally weaker than those between two hydrocarbons, then one might expect low hydrocarbon solubility in perfluorinated polymers. To explore this hypothesis, we present sorption data for C1−C3 saturated hydrocarbons and fluorocarbons as well as normal- and cyclo-C5 and -C6 alkanes in a rubbery, fluorinated, random copolymer containing 50.7 mol % tetrafluoroethylene (TFE) and 49.3 mol % perfluoromethyl vinyl ether (PMVE), TFE/PMVE49. The Sanchez−Lacombe equation of state is used to model the sorption data. The sorption results also show the effect of hydrocarbon−fluorocarbon interactions on the slope value, b, of the linear relationship between ln S and T_c (eq 1). N_2, CO_2, and C1−C3 hydrocarbon permeabilities in this polymer are also reported. The effect of hydrocarbon−fluorocarbon interactions on hydrocarbon permeabilities is discussed.

Background

Permeability. The permeability of a polymer film to a pure gas is given by[26]

$$P = \frac{Nl}{p_2 - p_1} \qquad (4)$$

where P is the permeability coefficient, N is the steady-state gas flux through the polymer membrane, l is film thickness, p_2 is the feed or upstream pressure, and p_1 is the permeate or downstream pressure. Penetrant transport through a polymer film is commonly described by a three-step solution−diffusion mechanism.[26] According to this mechanism, when penetrant flux obeys Fick's law and the downstream pressure is negligible relative to the upstream pressure, the permeability coefficient, P, can be expressed as[26]

$$P = SD \qquad (5)$$

where D is the effective concentration-averaged diffusion coefficient. S, the solubility coefficient at the upstream pressure, is the ratio of the equilibrium concentration of the penetrant in the polymer at the upstream face of the membrane to the upstream pressure. The effective concentration-averaged diffusivity is defined by[26]

$$D = \frac{1}{C_2 - C_1}\int_{C_1}^{C_2} \frac{D_{loc}}{1 - \omega}\, dC = \frac{1}{C_2 - C_1}\int_{C_1}^{C_2} D_{eff}\, dC \qquad (6)$$

where D_{loc} is the local concentration-dependent diffusion coefficient, ω is penetrant mass fraction in the polymer at concentration C, and D_{eff} is the so-called local effective diffusion coefficient.

Selectivity. The ideal selectivity, $\alpha_{A/B}$, of component A over B is a measure of the potential separation characteristics of the membrane material. The ideal selectivity can be written as the ratio of the pure gas

permeabilities:[26]

$$\alpha_{A/B} \equiv \frac{P_A}{P_B} \tag{7}$$

or

$$\alpha_{A/B} = \left(\frac{S_A}{S_B}\right)\left(\frac{D_A}{D_B}\right) \tag{8}$$

where the first term on the right-hand side of eq 8 is the solubility selectivity and the second is the diffusivity selectivity. In eqs 7 and 8, S_i, D_i, and P_i are the solubility, diffusivity, and permeability of gas i in the polymer, respectively.

Solubility. The uptake of vapors in a rubbery polymer is frequently described using the Flory−Huggins expression[32]

$$\ln a = \ln \phi_2 + (1 - \phi_2) + \chi(1 - \phi_2)^2 \tag{9}$$

where a is penetrant activity in the vapor phase, ϕ_2 is the volume fraction of sorbed penetrant, and χ is the Flory−Huggins interaction parameter. The Flory−Huggins equation is widely employed to model sorption in rubbery polymers due, in part, to its ease of use. However, it makes many approximations in describing thermodynamic properties of mixtures of small molecules with polymers, such as random mixing and absence of excess volume in the mixture. Many theories have been developed to take explicit account of some of these factors, though they are often more difficult to use than the Flory−Huggins model. For example, the Sanchez−Lacombe model is a lattice-based model that permits the presence of empty sites in the lattice, so that free volume exists in the polymer−penetrant mixture, and volume changes upon mixing penetrant and polymer molecules are allowed.[33]

The Sanchez−Lacombe (SL) model treats molecules as a set of connected segments on a lattice. In mixtures, the components are mixed randomly, like in the Flory−Huggins model.[34] Each component of the mixture is completely characterized by three independent parameters:[35] (i) P_i^*, the characteristic pressure, which is the hypothetical cohesive energy density of component i in the close-packed state (liquid at 0 K); (ii) ρ_i^*, which is the corresponding mass density in the close-packed state; and (iii) the characteristic temperature T_i^*, which is related to the depth of the potential energy well. These three parameters are determined from experimental pure component PVT data. A dimensionless size parameter, r_i^0, also appears in the following equations, and it is defined as follows:

$$r_i^0 = \frac{P_i^* M_i}{R T_i^* \rho_i^*} = \frac{M_i}{\rho_i^* v_i^*} \tag{10}$$

where R is the gas constant, M_i is the molecular weight, and v_i^* is the close-packed volume of a lattice site. Because r_i^0 represents the number of lattice sites occupied by a molecule, it is usually set to infinity for the polymer. The SL model provides equations of state for both pure components and mixtures as well as chemical potential expressions for each species. The chemical potential of the pure penetrant in the gaseous state could alternatively be expressed by other models, possibly more appropriate for a noncondensed phase. For simplicity, we use the SL model both for gaseous and polymeric phases. The solubility of a gas in a polymer is determined, at fixed temperature and pressure, by satisfying the equation-of-state properties of the pure penetrant gas phase and the polymer−penetrant mixture (eqs 11 and 12) and by equating the chemical potential of penetrant in both the penetrant and polymer phases (eq 13). In the following equations, variables with subscript 1 or 2 refer to the penetrant or the polymer, respectively.

$$\tilde{\rho}_1 = 1 - \exp\left[-\frac{\tilde{\rho}_1^{\,2}}{\tilde{T}_1} - \frac{\tilde{P}_1}{\tilde{T}_1} - \left(1 - \frac{1}{r_1^0}\right)\tilde{\rho}_1\right] \tag{11}$$

$$\tilde{\rho} = 1 - \exp\left[-\frac{\tilde{\rho}^2}{\tilde{T}} - \frac{\tilde{P}}{\tilde{T}} - \left(1 - \frac{\Phi_1}{r_1}\right)\tilde{\rho}\right] \tag{12}$$

$$\left[-\frac{\tilde{\rho}_1}{\tilde{T}_1} + \frac{\tilde{P}_1}{\tilde{T}_1\tilde{\rho}_1} + \frac{(1 - \tilde{\rho}_1)\ln(1 - \tilde{\rho}_1)}{\tilde{\rho}_1} + \frac{\ln \tilde{\rho}_1}{r_1^0}\right] r_1^0 = \ln \Phi_1 + (1 - \Phi_1) + \tilde{\rho}\frac{M_1}{\rho_1^*}\frac{\Delta P^*}{RT}(1 - \Phi_1)^2 + \left[-\frac{\tilde{\rho}}{\tilde{T}_1} + \frac{\tilde{P}_1}{\tilde{T}_1\tilde{\rho}} + \frac{(1 - \tilde{\rho})\ln(1 - \tilde{\rho})}{\tilde{\rho}} + \frac{\ln \tilde{\rho}}{r_1^0}\right] r_1^0 \tag{13}$$

In the equations above $\tilde{\rho}_1$, $\tilde{P}_1$, and $\tilde{T}_1$ are the reduced density, pressure, and temperature of the pure penetrant, and $\tilde{\rho}$, $\tilde{P}$, and $\tilde{T}$ are the corresponding variables for the mixture. Φ_1 is the close-packed volume fraction of gas in the polymer,[34] which is related to the mass fraction of gas dissolved in the polymer through eq 14.[36] The parameters r_1^0 and r_1 are the number of lattice sites occupied by a gas molecule in the pure gas and in the mixture, respectively. Penetrant solubility is determined by solving eqs 11, 12, and 13 simultaneously for $\tilde{\rho}_1$, $\tilde{\rho}$, and Φ_1. The equilibrium penetrant mass fraction, ω_1, is then calculated as follows:

$$\omega_1 = \frac{\Phi_1}{\Phi_1 + (1 - \Phi_1)\dfrac{\rho_2^*}{\rho_1^*}} \tag{14}$$

The reduced variables are related to the actual density, pressure, and temperature as follows:

$$\tilde{\rho}_1 = \frac{\rho_1}{\rho_1^*} \qquad \tilde{P}_1 = \frac{p}{P_1^*} \qquad \tilde{T}_1 = \frac{T}{T_1^*} \tag{15}$$

$$\tilde{\rho} = \frac{\rho}{\rho^*} \qquad \tilde{P} = \frac{p}{P^*} \qquad \tilde{T} = \frac{T}{T^*} \tag{16}$$

where ρ_1 and ρ are the actual densities of the pure penetrant phase and of the mixture, respectively, and p and T are the pressure and temperature. The mixture parameters are given by the following previously

established mixing rules:[34,36]

$$P^* = \Phi_1 P_1^* + \Phi_2 P_2^* - \Phi_1 \Phi_2 \Delta P^* \tag{17}$$

$$T^* = \frac{P^*}{\dfrac{\Phi_1 P_1^*}{T_1^*} + \dfrac{\Phi_2 P_2^*}{T_2^*}} \tag{18}$$

and

$$\frac{1}{\rho^*} = \frac{\omega_1}{\rho_1^*} + \frac{\omega_2}{\rho_2^*} \tag{19}$$

Also

$$v^* = \frac{RT^*}{P^*} = \frac{r_i^0}{r_i} v_i^* \tag{20}$$

Equation 20 is used to calculate the value of r_i, the number of lattice sites occupied by component i in the mixture.

At finite temperatures, the cohesive energy density in the SL model is nearly equal to $\tilde{\rho}^2 P^*$. Thus, P^* is a measure of the strength of intermolecular interactions. In eqs 13 and 17, the parameter ΔP^* is the net change in cohesive energy density upon mixing molecules 1 and 2 at 0 K:[34]

$$\Delta P^* = P_1^* + P_2^* - 2P_{12}^* \tag{21}$$

where P_{12}^* is characteristic of the mixture and, as a first approximation, P_{12}^* is often equated to the geometric mean of P_1^* and P_2^*. To account for deviations of the actual value of P_{12}^* from the geometric mean, an empirical, dimensionless mixing parameter, Ψ, is introduced:

$$P_{12}^* = \Psi \sqrt{P_1^* \, P_2^*} \tag{22}$$

When $\Psi = 1$, P_{12}^* is the geometric mean of P_1^* and P_2^*. The geometric mean was first introduced by London to model energetic interactions between nonpolar molecules of different species, and it is strictly obeyed only when the ionization potentials of the different molecules have similar values.[37] Using this approximation, the value of ΔP^* can be estimated "a priori" without using any gas−polymer mixture data, and the SL model is entirely predictive once the pure component (i.e., gas and polymer) parameters are determined from PVT studies. The mixture interaction energy can be represented either by ΔP^* or by Ψ since they are related through eqs 21 and 22.

Studies of the mixture behavior of small molecule solutions of hydrocarbons and fluorocarbons have shown that the geometric mean approximation overestimates hydrocarbon−fluorocarbon interaction energies.[38] For example, Dantzler-Siebert and Knobler found that interactions between hydrocarbons and fluorocarbons, when described by the Kihara potential, were 10% weaker than predicted using the geometric mean approximation.[39] Song et al. also found that use of the all-atom optimized potential for liquid simulations (OPLS-AA) model could not accurately predict thermodynamic properties of hydrocarbon−fluorocarbon mixtures if the geometric mean approximation was employed to determine unlike molecular interactions in the mixture. Relative to predictions of the geometric mean rule, a reduction of 10% in the interaction energy between a methane and a perfluoromethane molecule was required to bring the simulation results into agreement with experimental observations.[40] Several theories have been proposed to account for the weak interactions between fluorocarbons and hydrocarbons,[38] but no theory has yet been successful in fully explaining the underlying phenomena.[40]

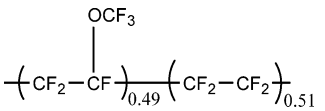

Figure 1. Chemical structure of TFE/PMVE49.

Similar results have been obtained by using gas−polymer mixtures containing hydrocarbon and fluorocarbon species. For example, as mentioned in the Introduction section, fluorocarbon gas−PDMS interactions require a Ψ value of ≈0.9 to have good agreement between the model and experimental gas sorption data.[31] Also, in the glassy perfluorinated polymers AF1600 and AF2400, modeling gas sorption using the nonequilibrium lattice fluid (NELF) equation of state provides good estimates of alkane solubility only if the value of P_{12}^* is reduced by ≈10% from its geometric mean value (i.e., $\Psi \approx 0.90$).[41] In contrast, good estimates of the solubility of perfluoroalkanes CF_4 and C_2F_6 in AF1600 and AF2400 are obtained with no adjustment to the geometric mean rule for the gas−polymer interactions (i.e., $\Psi = 1$).[41] The current study provides an opportunity to further investigate the unexpected behavior of these mixtures.

Diffusivity. The local effective diffusion coefficient, D_{eff}, is estimated from the slope of the sorption isotherm and the pressure dependence of permeability as follows:[42]

$$D_{\text{eff}}(C_2) = \left[P + \Delta p \left.\frac{\mathrm{d}P}{\mathrm{d}\Delta p}\right]_{p_2}\right] \left(\frac{\mathrm{d}p}{\mathrm{d}C}\right)_{p_2} \tag{23}$$

Experimental Section

Materials. TFE/PMVE49 was kindly provided by DuPont Dow Elastomers, L.L.C. (Wilmington, DE). The chemical structure of this amorphous perfluoroelastomer is shown in Figure 1. This random copolymer of TFE and PMVE was prepared by continuous emulsion polymerization by simultaneously feeding a gaseous mixture consisting of TFE (44.2 g/h) and PMVE (83.2 g/h) and an aqueous solution (243 mL/h) containing 0.91 g/L of ammonium persulfate, 6.17 g/L of disodium phosphate heptahydrate, and 50.62 g/L of ammonium perfluorooctanoate to a 1 L mechanically stirred autoclave. The temperature of the reaction was maintained at 85 °C and the pressure at 4.1 MPa (600 psi). The polymer emulsion was removed continuously by means of a letdown valve, and the unreacted monomers were vented.

The emulsion from 24 h of operation was collected, and the polymer was isolated by first diluting the emulsion with 8 volumes of deionized water per volume of emulsion at a temperature of 60 °C and then adding a solution of 75 g/L of magnesium sulfate heptahydrate to the diluted emulsion at the rate of 0.3 volume of the magnesium sulfate solution per volume of emulsion. After stirring for 1 h at 60 °C, the coagulated polymer crumb was filtered, washed in deionized water for 30 min at 45 °C, filtered again, and dried in an air oven for 48 h at 70 °C. The polymer yield was 3.7 kg. The composition of the polymer, as determined by FTIR, was 50.7 mol % TFE and 49.3 mol % PMVE. The polymer's inherent viscosity was 0.65 dL/g, as measured in a solution of 0.1 g of

polymer in 100 g of a solvent mixture consisting of 60/40/3 volume ratio of heptafluoro-2,2,3-trichlorobutane, perfluoro-(butyltetrahydrofuran), and ethylene glycol dimethyl ether at 30 °C.

Isotropic dense films of TFE/PMVE49 were prepared from a 2% (w/v) solution of the polymer in a volatile, fluorinated solvent, PF5060 (3M, Minneapolis, MN). The films were dried at ambient conditions. The polymer film density was determined independently by both laboratories participating in this study. The measured values were 1.99 g/cm^3 at the University of Texas at Austin and 2.02 g/cm^3 at the University of Bologna, both of which are close to the value of 2.0 g/cm^3 provided by the company. Using Bondi's group contribution method, the polymer has a fractional free volume of 0.22.[43] The glass transition temperature of this polymer is −8 °C as measured by a differential scanning calorimeter at a heating rate of 20 °C/min.

N_2, CO_2, CH_4, and C_2H_6 were obtained from National Specialty Gases (Raleigh, NC) and Matheson TriGas (Austin, TX), CF_4 and C_2F_6 from Scott Specialty Gases (Durham, NC) and Matheson TriGas (Austin, TX), and C_3H_8 and C_3F_8 from Machine and Welding (Raleigh, NC) and Matheson TriGas (Austin, TX). All gases had a purity of at least 99.5% and were used as received. For gas transport measurements performed at the University of Bologna, *n*-C_5H_{12}, *n*-C_6H_{14}, and c-C_5H_{10} were provided by Sigma-Aldrich and had a purity of at least 99.5, 99.5, and 99.0%, respectively. c-C_6H_{12} was provided by Carlo Erba Reagenti, Rodano (MI), Italy, and had a purity of at least 99.5%. The lower hydrocarbon and fluorocarbon gases were provided by SIAD SpA, Bergamo, Italy.

Sorption Measurements. Pure gas solubility coefficients at pressures above 1 atm were determined using a high-pressure barometric apparatus.[44] Initially, a polymer film was placed in the sample chamber and exposed to vacuum overnight to remove the air gases. A known amount of penetrant gas was introduced into the chamber, and the pressure was allowed to equilibrate. Once the chamber pressure was constant, the amount of gas sorbed by the polymer was determined by mass balance. Then additional penetrant was introduced and the procedure was repeated. In this incremental manner, penetrant uptake was determined as a function of pressure. The maximum pressure was 7−25 atm depending on the penetrant. After measuring each isotherm, the polymer samples were degassed under vacuum overnight. The system temperature was controlled to ±0.1 °C using a constant temperature water bath. The sorption experiments were performed in the order N_2, CO_2, CH_4, CF_4, C_2H_6, C_3H_8, C_2F_6, and C_3F_8. N_2 sorption was also measured after each of the other penetrants to determine whether the polymer film had undergone significant structural changes during the sorption process. Sorption experiments were continued only after the N_2 sorption isotherm matched the initially measured values.

Pure gas solubility coefficients at pressures below 1 atm were determined using a differential pressure decay device. This apparatus consists of a small cell, about 60 cm^3 in volume, in which the polymer sample was placed. This cell was initially exposed to vacuum to remove the air gases. The cell was connected to a larger vessel, about 2 L in volume, by a valve. The larger vessel was initially filled with a fixed amount of penetrant, and its pressure was measured using a Barocel capacitance manometer, with a full scale reading of 1000 mbar and an accuracy of 0.15% of full scale. For condensable penetrants, the vapor was generated in an evacuated bottle by evaporating liquid penetrant, while the noncondensable gases were fed into the vessel directly from a high-pressure cylinder. The whole apparatus was placed in a constant temperature enclosure, and the temperature was controlled to ±0.1 °C.

The sorption experiment was started by opening the connecting valve between the sample chamber and the larger vessel briefly (about 1−2 s) to rapidly equalize the pressures in the two volumes. The valve was then closed, and the pressure difference between the sample chamber and the vessel was monitored by a differential manometer (Druck LPM 9381) with a full scale of 10 mbar and an accuracy of at least

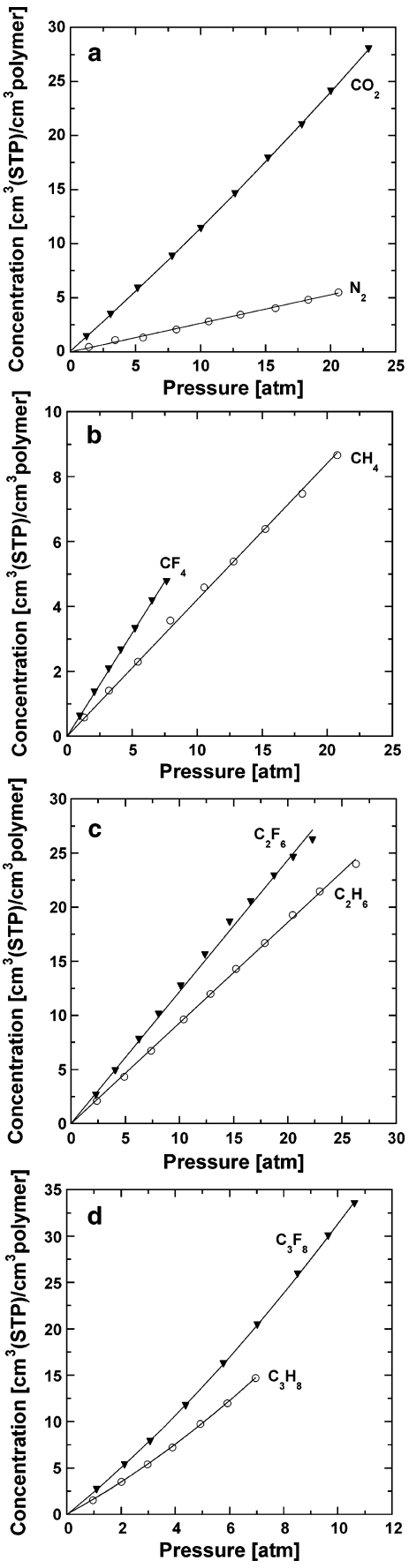

Figure 2. Sorption isotherms of (a) N_2 and CO_2, (b) CH_4 and CF_4, (c) C_2H_6 and C_2F_6, and (d) C_3H_8 and C_3F_8 in TFE/PMVE49 at 35 °C.

Table 3. Critical Temperatures of Hydrocarbon and Fluorocarbon Gases and Vapors[49]

gas/vapor	critical temp (K)	gas/vapor	critical temp (K)
CH_4	190.6	c-C_5H_{12}	511.8
C_2H_6	305.4	c-C_6H_{14}	553.6
C_3H_8	369.9	CF_4	227.6
n-C_5H_{12}	469.7	C_2F_6	293.0
n-C_6H_{14}	507.5	C_3F_8	345.1

±0.02 mbar. Since the pressure in the larger vessel was constant, the variation of the pressure difference with time was directly related to the moles of gas absorbed by the polymer. This procedure allows measurement of very small sorption levels due to the high accuracy of the differential manometer and the small volume of the sample chamber. Both equilibrium solubility and gas diffusion coefficients can be obtained from this experiment. For the calculation of mass uptake, the ideal gas equation of state is assumed to hold true for the gas phase in the sample chamber. The polymer samples were dried overnight under vacuum before the experiment.

Polymer Pressure−Volume−Temperature (PVT) Measurements. A Gnomix machine developed by Zoller and coworkers[45] was used to determine the pressure−volume−temperature properties of the copolymer. In this technique, the sample was held under hydrostatic mercury pressure, and the experiment was performed at fixed temperature by increasing the pressure in a stepwise fashion and recording the corresponding change in polymer volume. After completing an isothermal run, the system temperature was increased to the next higher temperature, and the pressure cycle was repeated. The accuracy of the Gnomix machine is ±0.002 cm^3/g in specific volume, up to 250 °C. The sensitivity is better than ±0.0005 cm^3/g. PVT experiments in this study were performed over a temperature range from 30 to 175 °C and at pressures ranging from 20 to 160 MPa.

Permeation Measurements. Pure gas permeability coefficients were measured in a constant volume/variable pressure apparatus.[46] The membrane area was 13.8 cm^2. The upstream pressure was varied from 2 to 15 atm. The downstream side was maintained below 10 mmHg. Prior to each experiment, the upstream and downstream sides of the permeation cell were evacuated to below 0.5 mmHg. The system temperature was controlled to ±0.5 °C using an Omega CN76000 temperature controller. The increase in pressure on the downstream side was recorded using a data acquisition system employing Labtech software. When the rate of pressure increase on the downstream side, dp/dt (cm Hg/s), attained its pseudo-steady-state value, the permeability (cm^3 (STP) cm/(cm^2 s cmHg)) was calculated using the expression

$$P = \frac{22414}{A}\frac{l}{p_{\mathrm{abs}}}\frac{V}{RT}\frac{\mathrm{d}p}{\mathrm{d}t} \tag{24}$$

where l is the membrane thickness (cm), A is the membrane area (cm^2), p_{abs} is the upstream pressure (cmHg), V is the downstream volume (cm^3), R is the universal gas constant (6236.56 cm^3 cmHg/(mol K)), and T is the absolute temperature (K).

Results and Discussion

Sorption Measurements. Figure 2a−d presents sorption isotherms of N_2, CO_2, and C1−C3 saturated hydrocarbon and fluorocarbon penetrants in TFE/PMVE49 at 35 °C. The isotherms for the lighter, low sorbing gases are linear while the higher sorbing penetrants exhibit isotherms that are convex to the pressure axis. This behavior is consistent with the generally expected nature of gas and vapor sorption isotherms in rubbery polymers.[47] Comparison of fluorocarbon and hydrocarbon gas/vapor sorption isotherms (Figure 2b−d) reveals that the hydrocarbon penetrants sorb less than their fluorocarbon analogues in TFE/PMVE49, which is consistent with previous reports of sorption in perfluorinated polymer matrices.[48] For the C1 penetrants, this trend is not unexpected since CF_4 has a higher critical temperature (T_c) than CH_4, and therefore, CF_4 is expected to be more soluble than CH_4 on the basis of the ln $S-T_c$ relationship (cf. Table 3 for T_c values[49]). However, C_2H_6 and C_3H_8 have higher critical temperatures than C_2F_6 and C_3F_8, respectively, thus indicating that factors other than condensability are also influencing the sorption process.

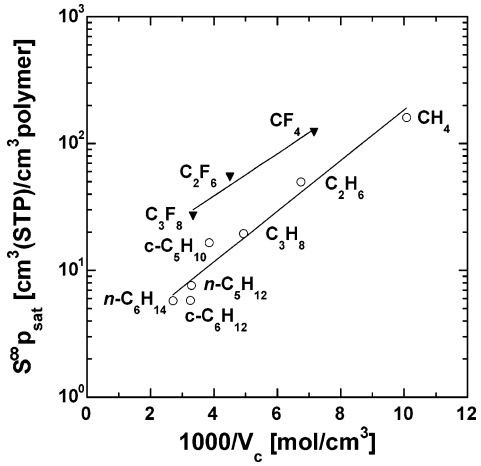

Figure 3. Condensability-normalized infinite dilution solubility of hydrocarbon and fluorocarbon penetrants in TFE/PMVE49 at 35 °C.

Figure 3 presents condensability-normalized infinite dilution solubility as a function of inverse penetrant critical volume. The infinite dilution solubility, S^{∞}, is defined as

$$S^{\infty} = \lim_{p\to 0}\frac{C}{p} \tag{25}$$

S^{∞} is determined by extrapolating the best-fit trendlines for gas solubility as a function of pressure to zero pressure. Presenting the data as shown in Figure 3 helps separate three principal factors governing penetrant sorption in a polymer: (i) penetrant condensability, (ii) penetrant size, and (iii) polymer−penetrant interactions.[30] For example, in the limit of infinite dilution, the Flory−Huggins model[32] can be written as follows:

$$S^{\infty}p_{\mathrm{sat}} = \frac{22414}{V_1\exp(1+\chi)} \tag{26}$$

where p_{sat}, the penetrant saturation pressure, is a measure of penetrant condensability; V_1, the penetrant partial molar volume, incorporates the effect of penetrant size; and χ, the Flory−Huggins interaction parameter, accounts for polymer−penetrant interactions. The left-hand side of this equation represents solubility that has been normalized for condensability effects. From eq 26, the condensability-normalized solubility is a function of penetrant size and polymer−penetrant interactions only. Thus, variations in the condensability-normalized solubility for penetrants of the same size should arise due to differences in the interactions of the two penetrants with the polymer matrix. Wong et al. pointed out that partial molar volumes often correlate linearly with gas critical vol-

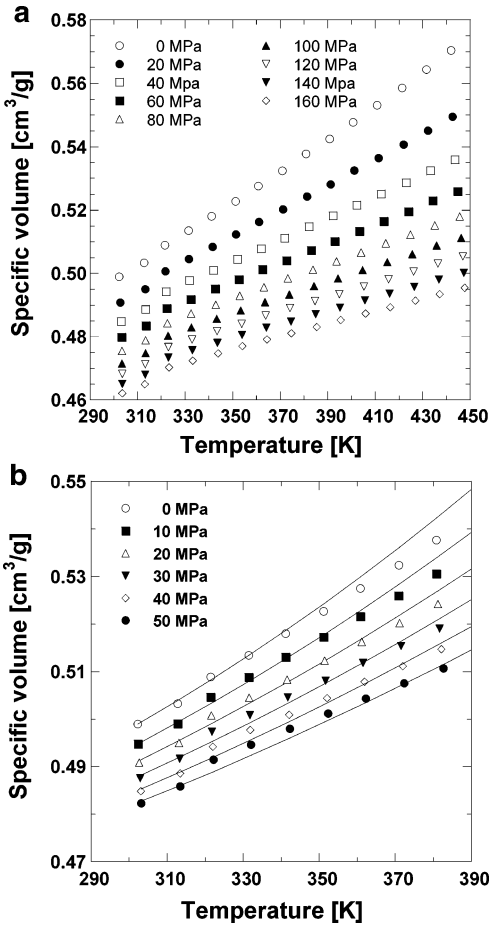

Figure 4. (a) Specific volume of TFE/PMVE49 as a function of temperature at various pressures (0−160 MPa). The zero-pressure values are extrapolated using the Tait equation.[51] (b) Experimental and calculated specific volume of TFE/PMVE49 as a function of temperature at various pressures (0−50 MPa). The zero-pressure values are extrapolated using the Tait equation.[51] The trendlines in the figure are fits to the data with the best fit parameters: $P^* = 395$ MPa, $T^* = 509$ K, $\rho^* = 2.244$ g/cm^3.

Table 4. Characteristic Parameters for the Sanchez−Lacombe Model

substance	P^* (MPa)	T^* (K)	ρ^* (g/cm^3)	source
TFE/PMVE49	395	509	2.244	PVT data [this work]
CH_4	250	215	0.500	31
C_2H_6	330	320	0.640	31
C_3H_8	320	375	0.690	31
n-C_5H_{12}	304	451	0.752	PVT data[54]
n-C_6H_{14}	298	476	0.770	55
c-C_5H_{12}	389	478	0.880	PVT data[54]
c-C_6H_{14}	383	497	0.902	55
CF_4	252	236	1.910	PVT data[54]
C_2F_6	260	280	2.050	PVT data[54]
C_3F_8	225	335	2.050	31

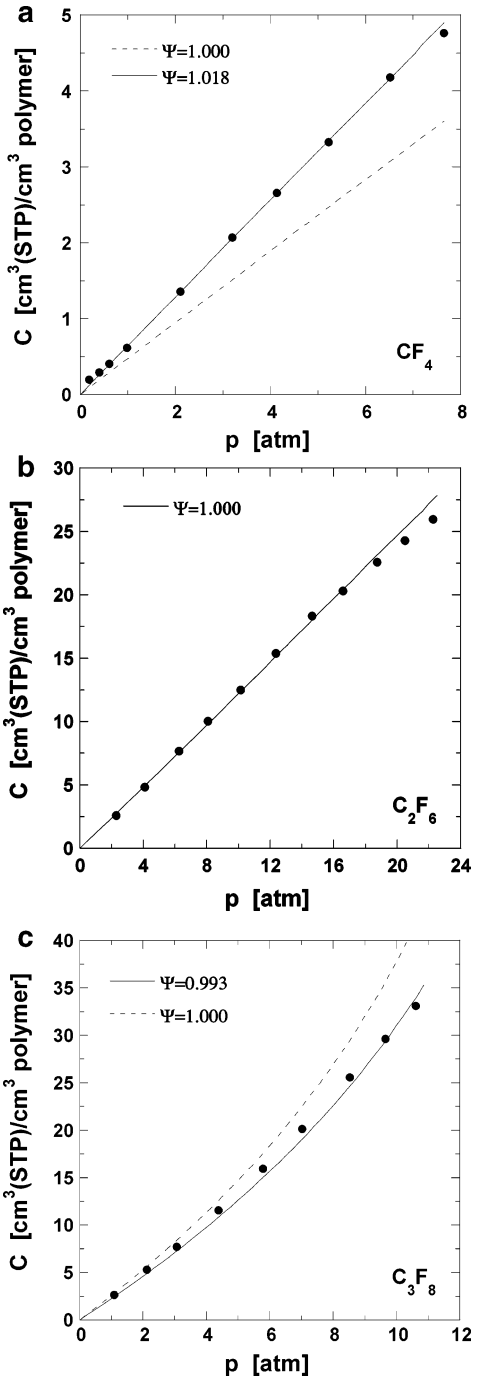

Figure 5. Experimental and calculated sorption isotherm of (a) CF_4, (b) C_2F_6, and (c) C_3F_8 in TFE/PMVE49 at 35 °C. The solid lines in each figure are calculated using the SL model with an adjustable binary parameter (best-fit values shown in each figure) while the dashed lines are obtained with the default value of the binary parameter ($\Psi = 1.000$).

umes,[50] so gas critical volume is used as a measure of penetrant size. From Figure 3, condensability-normalized solubilities of both fluorocarbons and hydrocarbons decrease with increasing penetrant size, consistent with more energy being required to open larger gaps in the polymer matrix to accommodate larger penetrants. However, at the same penetrant critical volume, hydrocarbon penetrants have a lower condensability-normalized solubility than fluorocarbon penetrants. On this basis, the interactions between hydrocarbon penetrants and the perfluorinated polymer are less favorable than those between the fluorinated penetrants and the perfluorinated polymer. This observation agrees with the report of lower fluorocarbon solubility in the hydrocarbon rubbery polymer, PDMS, due to hydrocarbon−fluorocarbon interactions.[29,30]

Sanchez−Lacombe Model. To calculate sorption isotherms for gas−polymer systems using the SL model, values of the characteristic parameters of the pure polymer and the pure gases are required. SL parameters for the polymer are determined by a least-squares regression of the SL model to experimental values of polymer density as a function of pressure and temper-

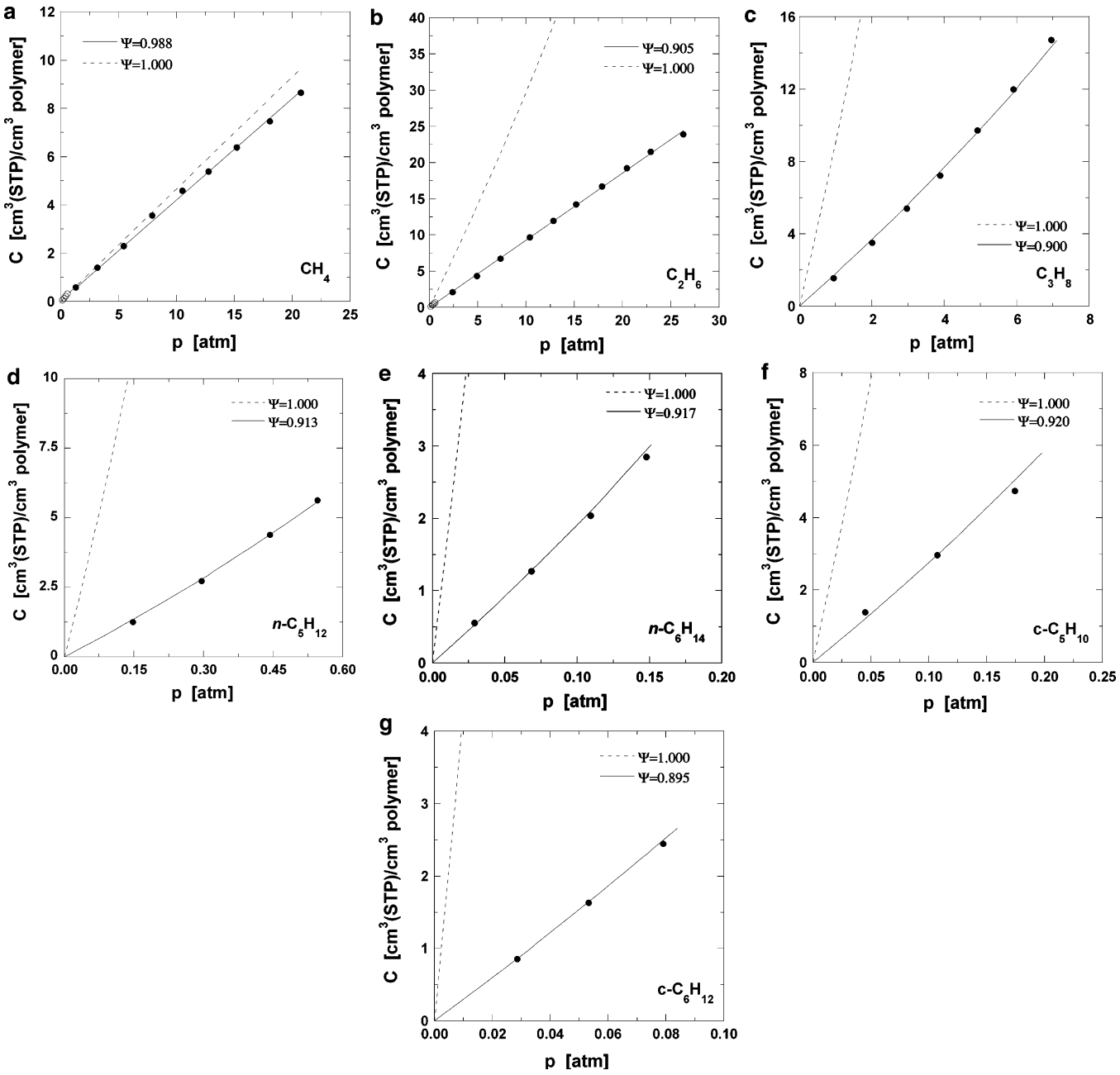

Figure 6. (a) Experimental and calculated sorption isotherm of CH_4 in TFE/PMVE49 at 35 °C. The solid and open symbols indicate experimental data measured above and below 1 atm, respectively, as described in the Experimental Section. The solid line is calculated using the SL model with $\Psi = 0.988$, while the dashed line is obtained with $\Psi = 1$. (b) Experimental and calculated sorption isotherm of C_2H_6 in TFE/PMVE49 at 35 °C. The solid and open symbols indicate experimental data measured above and below 1 atm, respectively, as described in the Experimental Section. The solid line is calculated using the SL model with $\Psi = 0.905$, while the dashed line is obtained with $\Psi = 1$. (c) Experimental and calculated sorption isotherm of C_3H_8 in TFE/PMVE49 at 35 °C. The solid line is calculated using the SL model with $\Psi = 0.900$, while the dashed line is obtained with $\Psi = 1$. (d) Experimental and calculated sorption isotherm of n-C_5H_{12} in TFE/PMVE49 at 35 °C. The solid line is calculated using the SL model with $\Psi = 0.913$, while the dashed line is obtained with $\Psi = 1$. (e) Experimental and calculated sorption isotherm of n-C_6H_{14} in TFE/PMVE49 at 35 °C. The solid line is calculated using the SL model with $\Psi = 0.917$, while the dashed line is obtained with $\Psi = 1$. (f) Experimental and calculated sorption isotherm of c-C_5H_{10} in TFE/PMVE49 at 35 °C. The solid line is calculated using the SL model with $\Psi = 0.920$, while the dashed line is obtained with $\Psi = 1$. (g) Experimental and calculated sorption isotherm of c-C_6H_{12} in TFE/PMVE49 at 35 °C. The solid line is calculated using the SL model with $\Psi = 0.895$, while the dashed line is obtained with $\Psi = 1$.

ature. In this study, polymer PVT data were determined over a wide range of temperatures (300−450 K) and pressures (0−160 MPa) and are presented in Figure 4a. (For the sake of clarity, data have been displayed in pressure increments of 20 MPa; data at intermediate pressures are not presented.) The values at zero pressure were determined by extrapolation using the Tait equation.[51] A single set of SL parameters often cannot accurately describe experimental PVT data over wide temperature and pressure ranges such as those explored in this study.[52,53] As the solubility values calculated using the SL model are rather sensitive to the polymer parameter values, it is important to choose a set of parameters that accurately describes the pure polymer volumetric properties in the temperature and pressure range of interest. When a comparison between experimental and predicted data is required at a specific temperature and over a narrow range of pressures, the

Table 5. Best-Fit Values of the Binary Parameter, Ψ, for Penetrants in TFE/PMVE49 at 35 °C

penetrant	Ψ	penetrant	Ψ	penetrant	Ψ
CF_4	1.018	C_2H_6	0.905	n-C_6H_{14}	0.917
C_2F_6	1.000	C_3H_8	0.900	c-C_5H_{12}	0.920
C_3F_8	0.993	n-C_5H_{12}	0.913	c-C_6H_{14}	0.895
CH_4	0.988				

most appropriate choice of polymer parameters is the set that provides the best description of the experimental PVT data of the polymer over the range of temperature and pressure of interest. Therefore, for the purposes of this study, we consider a temperature range from 300 to 380 K and a pressure range from 0 to 50 MPa, which encompasses the temperature and pressure range of the sorption data. This truncated PVT data set is shown in Figure 4b. The best fit SL parameter values for this data set are recorded in Table 4, and predictions of the SL model with these parameter values are shown by solid lines in Figure 4b. The SL model predictions of the polymer specific volume are within ±1.5% of the experimental values. SL parameters for the pure gases were determined in a similar manner by least-squares fits to experimental PVT data reported in the literature,[31,54,55] and they are also recorded in Table 4.

Figure 5a−c presents SL model fits to C1−C3 fluorocarbon penetrant sorption in TFE/PMVE49 with Ψ = 1 and with Ψ treated as an adjustable parameter. From the figures, the SL model fit with Ψ = 1 provides a good fit to C_2F_6 sorption data, while it underestimates CF_4 solubility and slightly overestimates C_3F_8 solubility. A 1.8% increase in the Ψ value for CF_4 is required to fit the low- and high-pressure data satisfactorily, while a 0.7% decrease in Ψ models the C_3F_8 sorption isotherm adequately. Thus, the geometric mean approximation, with minor adjustments, is sufficient to provide a reasonable prediction of fluorocarbon solubility in this fluoropolymer. This finding agrees with previous observations of the general applicability of the geometric mean approximation to model gas sorption in chemically similar gas−polymer systems (i.e., fluorocarbon gas sorption in fluoropolymers and hydrocarbon gas sorption in hydrocarbon polymers).[31,41]

Figure 6a−g presents SL fits with the default Ψ value (1.0) and with adjustable Ψ values for C1−C3 hydrocarbon penetrants as well as normal- and cyclo-C5 and -C6 alkanes. The data for the C5 and C6 compounds have been measured at subatmospheric pressures by the pressure decay technique, while C1−C3 penetrant sorption was measured in the high-pressure barometric apparatus. To provide a comparison between the sorption values determined by the two techniques, sorption of CH_4 and C_2H_6 were also measured in the subatmospheric range, and the results are shown in parts a and b of Figure 6, respectively. There is satisfactory agreement between the data obtained by these two techniques.

From Figure 6a−g, except for CH_4, sorption of hydrocarbon penetrants is significantly overpredicted when the SL model utilizes the geometric mean approximation. CH_4 sorption is only slightly overpredicted by the SL model with Ψ = 1, and it is adequately described with a minor change in the binary parameter (Ψ = 0.988). However, SL model predictions of sorption isotherms of higher hydrocarbons with Ψ = 1 are 3−18 times higher than the experimentally determined isotherms. It is not clear why CH_4 sorption is close to the geometric mean rule estimate while the higher hydrocarbons show substantial deviation. When the SL equation of state is used to model sorption of higher hydrocarbons with Ψ as an adjustable parameter, a reduction of ≈10% in the Ψ value is required to satisfactorily model the sorption isotherms of the higher hydrocarbons. (The exact Ψ values for each penetrant are recorded in Table 5.) This finding implies that the interaction energy between (higher) hydrocarbons and fluorocarbons is 10% weaker than that estimated from the geometric mean rule. This result is in good agreement with previous modeling reports of sorption in hydrocarbon−fluorocarbon gas−polymer systems in rubbery[31] as well as glassy polymers.[41] Modeling small molecule solution behavior of hydrocarbon−fluorocarbon mixtures has also revealed a similar deviation of the unlike molecular interaction energies from the geometric mean value, as indicated in the background section.[39,40]

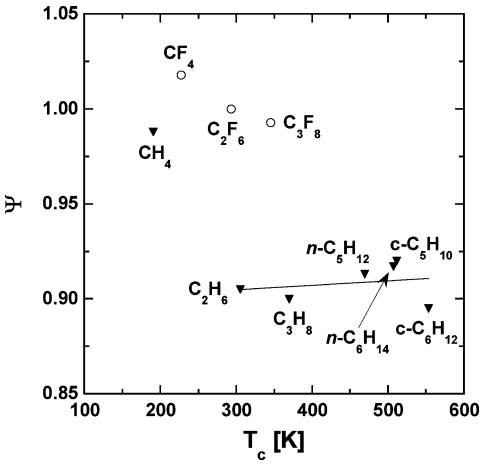

Figure 7. Best fit binary parameter values of the SL model for hydrocarbon and fluorocarbon penetrants.

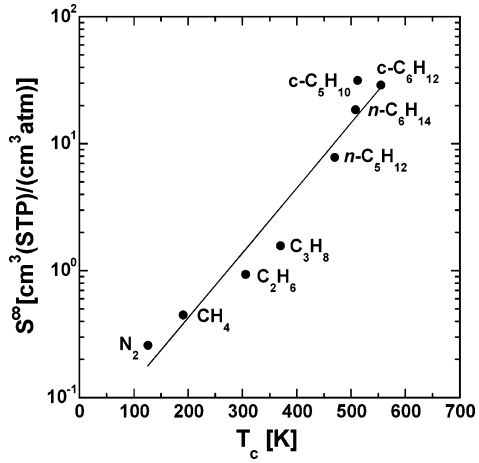

Figure 8. Infinite dilution solubility of N_2 and C1−C3, C5, and C6 hydrocarbons in TFE/PMVE49 at 35 °C as a function of penetrant critical temperature. The best-fit trendline through the experimental data is $\ln S^{\infty}$ [cm^3 (STP)/(cm^3 atm)] = −2.96 + 0.011T_c [K].

Figure 7 displays the best-fit Ψ values for all penetrants considered in this study as a function of their critical temperature. The Ψ value for fluorocarbon penetrants, as well as for CH_4, is close to the default value of 1.0, indicating the general applicability of the geometric mean approximation for these penetrants in TFE/PMVE49. However, the Ψ value for higher hydrocarbons is uniformly around 0.9, and it shows no

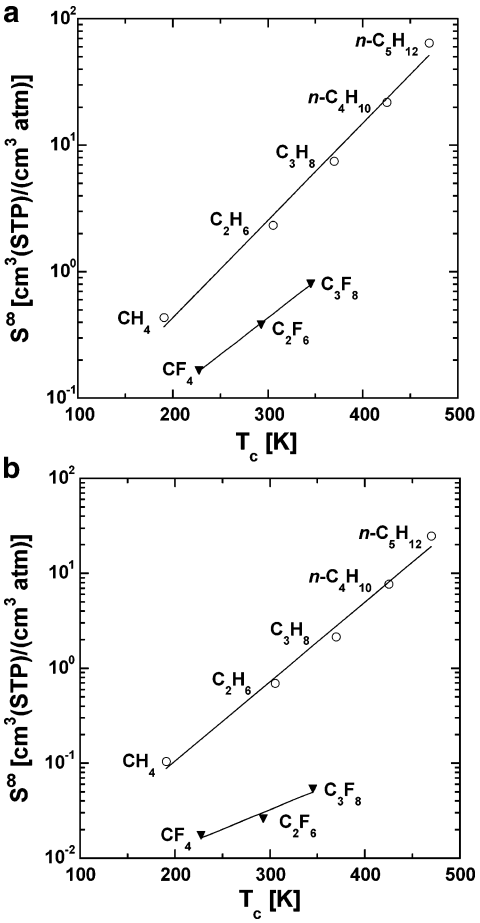

Figure 9. (a) Infinite dilution solubility coefficients of C1−C5 linear alkanes and C1−C3 fluorocarbons in PDMS at 25 °C as a function of penetrant critical temperature.[20] The best-fit trendlines through the experimental data are ln S^{∞} [cm^3 (STP)/(cm^3 atm)] = −4.37 + 0.018T_c [K] for the hydrocarbons and ln S^{∞} [cm^3 (STP)/(cm^3 atm)] = −4.85 + 0.013T_c [K] for the fluorocarbons. (b) Infinite dilution solubility coefficients of C1−C5 linear alkanes and C1−C3 fluorocarbons in LDPE at 25 °C as a function of penetrant critical temperature.[20] The best-fit trendlines through the experimental data are ln S^{∞} [cm^3 (STP)/(cm^3 atm)] = −6.12 + 0.019T_c [K] for the hydrocarbons and ln S^{∞} [cm^3 (STP)/(cm^3 atm)] = −6.27 + 0.009T_c [K] for the fluorocarbons.

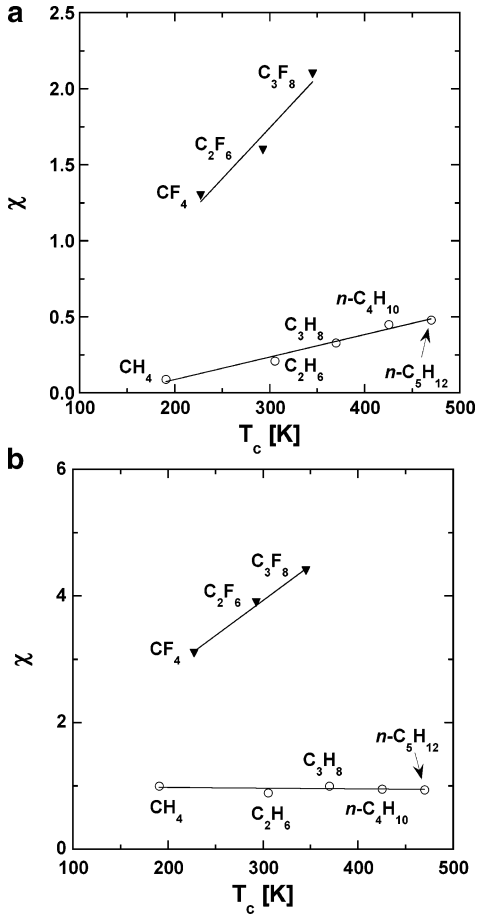

Figure 10. (a) χ values of C1−C5 linear alkanes and C1−C3 fluorocarbons in PDMS at 25 °C as a function of penetrant critical temperature.[20] The best-fit trendlines through the experimental data are $\chi = -0.2 + 0.0015T_c$ [K] for the hydrocarbons and $\chi = -0.27 + 0.0067T_c$ [K] for the fluorocarbons. (b) χ values of C1−C5 linear alkanes and C1−C3 fluorocarbons in LDPE at 25 °C as a function of penetrant critical temperature.[20] The best-fit trendlines through the experimental data are $\chi = 0.99 - 0.0001T_c$ [K] for the hydrocarbons and $\chi = 0.59 + 0.011T_c$ [K] for the fluorocarbons.

discernible systematic variation with the number of carbon atoms in the molecules or molecular shape (i.e., normal alkanes vs cycloalkanes). Thus, the weaker intermolecular interactions between hydrocarbons and fluorocarbons seem to be a consequence of specific interactions between the chemical species; molecular shape or size differences seem to be less important in causing deviations in intermolecular interactions from their geometric mean estimates. This result is in agreement with a recent report by Song et al. which showed that taking detailed account of molecular geometries through the OPLS-AA model was insufficient to describe methane−perfluoromethane mixture thermodynamic behavior if the geometric mean rule was employed to estimate the mixture interaction energy.[40]

Solubility Correlations. Figure 8 presents infinite dilution solubility coefficients of N_2, C1−C3, C5, and C6 linear alkanes in TFE/PMVE49 as a function of critical temperature. As discussed earlier, gas solubility in polymers correlates well with measures of penetrant condensability such as critical temperature. The slope of the linear relation between ln S and T_c is expected to have a value of 0.019 K^{-1} at 35 °C, based on theoretical considerations (eq 3), and experimental data for a wide variety of polymers provide best fit slope values within a narrow range around this value (cf. Table 2). However, the least-squares best fit straight line to the data in Figure 8 has a significantly lower slope value (0.011 K^{-1}). Therefore, with increasing condensability, hydrocarbon solubility in TFE/PMVE49 increases much less than in typical hydrocarbon polymers such as those listed in Table 2. Such a difference in slopes is also seen for fluorocarbon gas sorption in hydrocarbon polymers like PDMS and low-density poly(ethylene) (LDPE) (cf. Figure 9a,b). Gee's correlation (eq 2), in its present form, does not predict this difference in slope at constant temperature (cf. eq 3). However, eq 2 assumes that the polymer−penetrant interaction parameter, χ, varies negligibly from penetrant to penetrant and, therefore, can be assigned a constant value. Experimental results of gas sorption in polymers show that χ can vary significantly among penetrants of the same chemical family sorbing in a polymer. Figure 10a,b presents χ values of hydrocarbon and fluorocarbon linear alkanes in PDMS and LDPE.[20] From these figures, in both hydrocarbon polymers, the fluorocarbon penetrants have higher χ values than the hydrocarbons at the same critical temperature due, presumably, to less favorable interactions of fluorocarbons with the

Table 6. Comparison of Slope of ln $S-T_c$ Trendlines for Gas Sorption in Polymers with Theoretical Predictions from Eqs 3 and 28

polymer	penetrants	χ_0	χ_1	original slope (eq 3)[a]	modified slope (eq 28)	slope from exptl data
PDMS[20]	hydrocarbons	−0.20	0.0015	0.020	0.019	0.018
	fluorocarbons	−0.27	0.007	0.020	0.013	0.013
LDPE[20]	hydrocarbons	0.99	−0.0001	0.020	0.020	0.019
	fluorocarbons	0.59	0.011	0.020	0.009	0.009
TFE/PMVE49	hydrocarbons	−1.39 ± 0.02	0.0077 ± 0.0001	0.019	0.0113	0.011 ± 0.0003

[a] T = 35 °C for TFE/PMVE49 data and 25 °C for the other data.

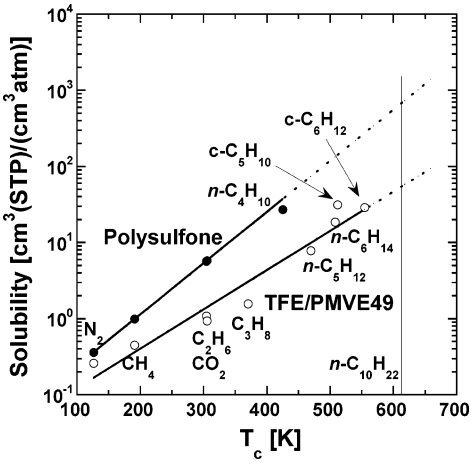

Figure 11. Solubility of N_2 and C1−C6 hydrocarbons in polysulfone[21] and TFE/PMVE49 at 35 °C as a function of penetrant critical temperature. The polysulfone data are at 10 atm except for n-C_4H_{10}, which is at infinite dilution. The data for TFE/PMVE49 have been extrapolated to infinite dilution conditions. The vertical line at a T_c value of 617.7 K corresponds to the critical temperature of n-decane.

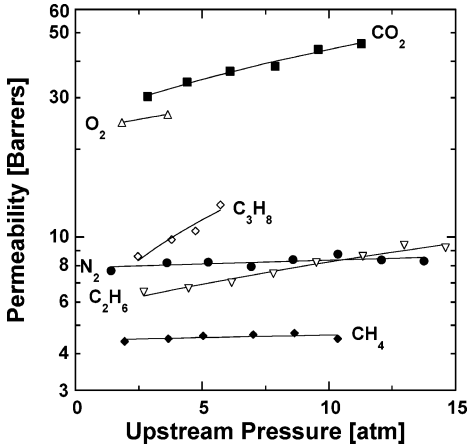

Figure 12. Permeabilities of N_2, O_2, CO_2, and C1−C3 saturated hydrocarbons in TFE/PMVE49 at 35 °C. The downstream pressure was very low (less than 10 mmHg).

hydrocarbon polymers. Also, the χ parameter shows much more variation with increasing carbon number in the fluorocarbon family than in the hydrocarbon family. One way to modify Gee's correlation is to take account of the observed variation in χ with penetrant condensability within a family of penetrants. From Figure 10a,b, the dependence of χ on penetrant critical temperature is linear and can be empirically described as

$$\chi = \chi_0 + \chi_1 T_c \tag{27}$$

where χ_0 and χ_1 are adjustable constants. χ_0 and χ_1 are determined from the linear best-fit trendline to experimental χ values as a function of T_c within a family of penetrants (e.g., hydrocarbons, fluorocarbons, etc.). Gee's correlation (eq 2) can be modified by using eqs 3 and 27 as follows:

$$\ln S = -(4.5 + \chi_0) + \left(\frac{6}{T} - \chi_1\right)T_c \tag{28}$$

The best-fit values of χ_0 and χ_1 for hydrocarbon and fluorocarbons in PDMS and LDPE and for hydrocarbon sorption in TFE/PMVE49 are listed in Table 6. From Table 6, taking account of the empirical dependence of χ on T_c brings the predicted slope in agreement with the slope obtained by fitting experimental solubility data for these polymers.

The lower slope for hydrocarbons in TFE/PMVE49 also implies that, for extremely large hydrocarbons, the differences in hydrocarbon solubility between this polymer and a polymer with a slope of ≈0.019 K^{-1} can be very large. One example is shown in Figure 11, which compares the ln $S-T_c$ relationship of polysulfone, a commercial membrane polymer, which has a slope value of 0.017 K^{-1}, with that of TFE/PMVE49. If the trendlines in the figure are valid beyond the range of presently available experimental data, then for a very large hydrocarbon like n-decane, having a critical temperature of 617.7 K, the difference in solubility in the two polymers is estimated to be over an order of magnitude, with the fluoropolymer exhibiting lower solubility. This significantly lower solubility for higher hydrocarbons might be useful in developing stable membranes for use in hydrocarbon environments, for example, in carbon dioxide removal from natural gas. Current hydrocarbon-based polymers undergo plasticization due to high solubility of large hydrocarbons present in natural gas streams, thus losing their high CO_2/CH_4 selectivity to a significant extent.[3,56] Polymers which have low hydrocarbon solubility may be less susceptible to plasticization in hydrocarbon environments than hydrocarbon-based polymers, and they may, therefore, provide more stable membranes for applications such as olefin/paraffin separation and natural gas purification.[57−59]

Permeability. The permeabilities of N_2, O_2, CO_2, and C1−C3 alkanes in TFE/PMVE49 at 35 °C are presented in Figure 12. N_2, O_2, and CH_4 exhibit constant permeabilities at all upstream pressures tested, while the permeabilities of CO_2, C_2H_6, and C_3H_8 increase with increasing upstream pressure. This result is consistent with the behavior of permanent gases and higher condensability penetrants in other rubbery polymers, e.g., PDMS.[29] However, the selectivities of PDMS for hydrocarbons over a permanent gas like N_2 are much higher than in TFE/PMVE49. Table 7 shows the ratios of hydrocarbon to N_2 selectivity values, calculated from infinite dilution permeabilities, in these two polymers. The ratio of infinite dilution solubility selectivities and diffusivity selectivities are also shown to demonstrate the source of the difference in overall selectivity in the

Table 7. Hydrocarbon/Nitrogen Permselectivity, Solubility Selectivity, and Diffusivity selectivity in PDMS[29] and TFE/PMVE49 at 35 °C

	TFE/PMVE49			PDMS		
gas	$P/P(N_2)$	$S/S(N_2)$	$D/D(N_2)$	$P/P(N_2)$	$S/S(N_2)$	$D/D(N_2)$
CH_4	0.56	1.7	0.33	3.0	4.7	0.64
C_2H_6	0.71	3.6	0.20	8.3	24	0.34
C_3H_8	0.72	6.1	0.12	10.3	56	0.18

Table 8. Infinite Dilution Solubilities, Permeabilities, and Diffusivities of Permanent Gases and Linear Alkanes in TFE/PMVE49

penetrant	S^∞ (cm^3 (STP)/(cm^3 atm)	P^∞ (barrers)	$D^\infty \times 10^8$ (cm^2/s)
N_2	0.3 ± 0.03	7.8 ± 0.6	23 ± 2
CO_2	1.1 ± 0.03	25.4 ± 3	18 ± 1.4
CH_4	0.45 ± 0.03	4.4 ± 0.3	7.5 ± 0.5
C_2H_6	0.9 ± 0.04	5.6 ± 0.9	4.5 ± 0.5
C_3H_8	1.6 ± 0.13	5.7 ± 2	3.6 ± 0.4
n-C_5H_{12}	7.9 ± 1.1		0.5 ± 0.1
n-C_6H_{14}	18.6 ± 2.1		0.5 ± 0.07

two polymers. Infinite dilution permeability values for N_2, CO_2, and C1−C3 hydrocarbons were obtained by extrapolating the trendlines through the permeability data for each penetrant in Figure 12 to zero upstream pressure. Similarly, infinite dilution solubility coefficients for N_2, CO_2, and C1−C3, C5, and C6 alkanes were calculated by extrapolating experimental penetrant solubilities as a function of pressure to zero pressure. Diffusion coefficients of N_2, CO_2, and C1−C3 hydrocarbons were determined as a function of pressure by using eq 23 and the solubility and permeability data. By extrapolating the diffusion coefficient data to zero pressure, infinite dilution diffusion coefficients were calculated for these penetrants. For C5 and C6 alkanes, infinite dilution diffusion coefficients were calculated by extrapolation from experimental diffusivity data as a function of pressure to zero pressure. Infinite dilution solubilities, permeabilities, and diffusivities of N_2, CO_2, and the linear alkanes are recorded in Table 8.

From Table 7, solubility selectivity differences play a major role in the overall hydrocarbon/N_2 selectivity differences in the two polymers. For example, propane/N_2 selectivity is more than an order of magnitude higher in PDMS than in TFE/PMVE49 due to nearly an order of magnitude difference in the solubility selectivity. The propane/N_2 diffusivity selectivity of TFE/PMVE49 is only a third lower than that of PDMS. Thus, the suppression of hydrocarbon solubility in the fluoropolymer, due to weak hydrocarbon−fluorocarbon interactions, plays a major role in influencing gas transport through the polymer.

Diffusivity. Infinite dilution diffusion coefficients of gases in TFE/PMVE49 are presented in Figure 13 as a function of penetrant critical volume. Diffusion coefficients of gases in a rubbery polymer (PDMS) and in a typical glassy polymer (polysulfone) are also presented to compare the size-sieving ability of TFE/PMVE49 with that of commercial gas and vapor separation membrane materials. From Figure 13, diffusion coefficients in polysulfone decrease by nearly 6 orders of magnitude from helium (V_c = 57.4 cm^3/mol) to n-butane (V_c = 255 cm^3/mol), while in PDMS, the decrease in diffusion coefficients is only about 2 orders of magnitude over the same penetrant range. Thus, polysulfone has a much greater size-sieving ability than PDMS, which translates into high selectivities for smaller gases over larger gases. From the figure, the size-sieving ability or diffusivity selectivity of TFE/PMVE49 is closer to that of rubbery PDMS than that of glassy polysulfone.

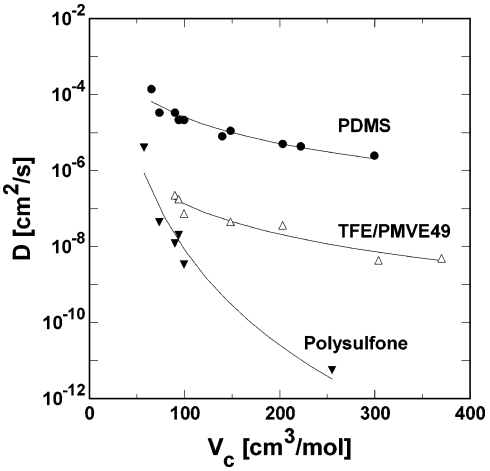

Figure 13. Comparison of the variation of infinite dilution diffusion coefficients with penetrant critical volume in TFE/PMVE49 with that in a typical rubbery (PDMS) and glassy (polysulfone) polymer. The trendlines in the figure satisfy the equation $D = \tau V_c^{-\eta}$, where η is a measure of the size-sieving ability or size selectivity of the polymer to penetrants. The best-fit values of η in the plot are as follows: PDMS, 2.3; polysulfone, 8.4; TFE/PMVE49, 2.6 ± 0.1. The best-fit value of τ for TFE/PMVE49 is 2.33×10^{-2} [(cm^2/s) (cm^3/mol)$^\eta$].

The variation of diffusion coefficients with critical volume (a measure of penetrant size) is often described by the empirical equation[60]

$$D = \frac{\tau}{V_c^{\eta}} \tag{29}$$

where τ and η are adjustable parameters. η provides a measure of the rate of decrease of diffusion coefficients with increasing penetrant size; the higher the value of η, the greater the diffusivity selectivity of the polymer. From Figure 13, the η values of PDMS and polysulfone are 2.3 and 8.4, respectively, indicating the much greater size-sieving ability of polysulfone. TFE/PMVE49 has an η value of 2.6, based on the best-fit trendline through the data in Figure 13, much lower than the η value of polysulfone.

Conclusions

C1−C3 hydrocarbons exhibit lower sorption in TFE/PMVE49 than their corresponding fluorocarbon analogues due to less favorable interactions of the fluorinated polymer matrix with the hydrocarbon penetrants as compared to the fluorocarbon penetrants. The slope of the linear correlation between natural logarithm of gas solubility and gas critical temperature is 0.011 K^{-1}, which is much lower than that exhibited by other polymers as well as that expected on the basis of a thermodynamic model by Gee. The lower slope is a consequence of hydrocarbon solubility suppression due to fluorocarbon−hydrocarbon interactions. The hydrocarbon−fluorocarbon interactions play a major role in influencing hydrocarbon penetrant permeation through this fluoropolymer. This polymer exhibits a size-sieving ability similar to that of a rubbery polymer like PDMS.

Acknowledgment. The authors are grateful for partial support of this work by the Chemical Sciences, Geosciences and Biosciences Division, Office of Basic

Energy Sciences, Office of Science, U.S. Department of Energy (DE-FG03-02ER15362), and by the University of Bologna (Progetto Pluriennale E.F. 2004/2005). The authors are also thankful to Professor Pavan of the Dipartimento di Chimica, Materiali e Ingegneria Chimica "Giulio Natta", Politecnico di Milano, Italy, for providing access to a dilatometer and to Dr. Francesco Briatico for performing the PVT measurements.

References and Notes

(1) Koros, W. J.; Fleming, G. K. *J. Membr. Sci.* **1993**, *83*, 1−80.
(2) Stern, S. A. *J. Membr. Sci.* **1994**, *94*, 1−65.
(3) White, L. S.; Blinka, T. A.; Kloczewski, H. A.; Wang, I.-F. *J. Membr. Sci.* **1995**, *103*, 73−82.
(4) Koros, W. J.; Hellums, M. W. *Fluid Phase Equilib.* **1989**, *53*, 339−354.
(5) Semenova, S. I.; Ohya, H.; Smirnov, S. I. *J. Membr. Sci.* **1997**, *136*, 1−11.
(6) Semenova, S. I.; Smirnov, S. I. *J. Membr. Sci.* **2000**, *168*, 167−173.
(7) Chiou, J. S.; Barlow, J. W.; Paul, D. R. *J. Appl. Polym. Sci.* **1985**, *30*, 2633−2642.
(8) Houde, A. Y.; Kulkarni, S. S.; Kulkarni, M. G. *J. Membr. Sci.* **1992**, *71*, 117−128.
(9) Sanders, E. S. *J. Membr. Sci.* **1988**, *37*, 63−80.
(10) Zhou, S.; Stern, S. A. *J. Polym. Sci., Part B: Polym. Phys.* **1989**, *27*, 205−222.
(11) Wessling, M.; Schoeman, S.; Boomgaard, T. v. d.; Smolders, C. A. *Gas Sep. Purif.* **1991**, *5*, 222−228.
(12) Petropoulos, J. H. *J. Membr. Sci.* **1992**, *75*, 47−59.
(13) Semenova, S. I.; Smirnov, S. I.; Ohya, H. *J. Membr. Sci.* **2000**, *172*, 75−89.
(14) van Amerongen, G. J. *J. Polym. Sci.* **1950**, *5*, 307−332.
(15) Gee, G. *Q. Rev. (London)* **1947**, *1*, 265−298.
(16) van Krevelen, D. W. *Properties of Polymers: Their Correlation with Chemical Structure; their Numerical Estimation and Prediction from Additive Group Contributions*, 3rd ed.; Elsevier: Amsterdam, 1990.
(17) Michaels, A. S.; Bixler, H. J. *J. Polym. Sci.* **1961**, *50*, 393−412.
(18) Barrer, R. M.; Skirrow, G. *J. Polym. Sci.* **1948**, *3*, 564−575.
(19) Korosy, F. *Trans. Faraday Soc.* **1937**, *33*, 416−425.
(20) Kamiya, Y.; Naito, Y.; Terada, K.; Mizoguchi, K. *Macromolecules* **2000**, *33*, 3111−3119.
(21) Ghosal, K.; Chern, R. Y.; Freeman, B. D.; Savariar, R. *J. Polym. Sci., Part B: Polym. Phys.* **1995**, *33*, 657−666.
(22) Toi, K.; Morel, G.; Paul, D. R. *J. Appl. Polym. Sci.* **1982**, *27*, 2997−3005.
(23) Serad, G. E.; Freeman, B. D.; Stewart, M. E.; Hill, A. J. *Polymer* **2001**, *42*, 6929−6943.
(24) Felder, R. M.; Rousseau, R. W. *Elementary Principles of Chemical Processes*, 2nd ed.; John Wiley and Sons: New York, 1986.
(25) Shah, V. M.; Hardy, B. J.; Stern, S. A. *J. Polym. Sci., Part B: Polym. Phys.* **1986**, *24*, 2033−2047.
(26) Ghosal, K.; Freeman, B. D. *Polym. Adv. Technol.* **1994**, *5*, 673−697.
(27) Lin, H.; Freeman, B. D. *J. Membr. Sci.* **2004**, *239*, 105−117.
(28) Lin, H.; Freeman, B. D. *J. Mol. Struct.*, in press.
(29) Merkel, T. C.; Bondar, V. I.; Nagai, K.; Freeman, B. D.; Pinnau, I. *J. Polym. Sci., Part B: Polym. Phys.* **2000**, *38*, 415−434.
(30) Merkel, T. C.; Bondar, V.; Nagai, K.; Freeman, B. D. *Macromolecules* **1999**, *32*, 370−374.
(31) De Angelis, M.-G.; Merkel, T. C.; Bondar, V. I.; Freeman, B. D.; Doghieri, F.; Sarti, G. C. *J. Polym. Sci., Part B: Polym. Phys.* **1999**, *37*, 3011−3026.
(32) Flory, P. *Principles of Polymer Chemistry*; Cornell University Press: Ithaca, NY, 1953.
(33) Sanchez, I. C.; Lacombe, R. H. *J. Phys. Chem.* **1976**, *80*, 2352−2362.
(34) Sanchez, I. C.; Lacombe, R. H. *Macromolecules* **1978**, *11*, 1145−1156.
(35) Sanchez, I. C. *Polymer* **1989**, *30*, 471−475.
(36) Pope, D. S.; Sanchez, I. C.; Koros, W. J.; Fleming, G. K. *Macromolecules* **1991**, *24*, 1779−1783.
(37) Prausnitz, J. M.; Lichtenthaler, R. N.; de Azevedo, E. G. *Molecular Thermodynamics of Fluid-Phase Equilibria*, 3rd ed.; Prentice Hall: Upper Saddle River, NJ, 1999.
(38) Scott, R. L. *J. Phys. Chem.* **1958**, *62*, 136−145.
(39) Dantzler-Siebert, E. M.; Knobler, C. M. *J. Phys. Chem.* **1971**, *75*, 3863−3870.
(40) Song, W.; Rossky, P. J.; Maroncelli, M. *J. Chem. Phys.* **2003**, *119*, 9145−9162.
(41) De Angelis, M.-G.; Merkel, T. C.; Bondar, V. I.; Freeman, B. D.; Doghieri, F.; Sarti, G. C. *Macromolecules* **2002**, *35*, 1276−1288.
(42) Stern, S. A.; Shah, V. M.; Hardy, B. J. *J. Polym. Sci., Part B: Polym. Phys.* **1987**, *25*, 1263−1298.
(43) Bondi, A. *Physical Properties of Molecular Crystals, Liquids and Glasses*; Wiley: New York, 1968.
(44) Bondar, V. I.; Freeman, B. D.; Pinnau, I. *J. Polym. Sci., Part B: Polym. Phys.* **1999**, *37*, 2463−2475.
(45) Zoller, P.; Bolli, P.; Pahud, V.; Ackerman, V. *Rev. Sci. Instrum.* **1976**, *47*, 948−952.
(46) Felder, R. M.; Huvard, G. S. In *Methods of Experimental Physics*; Fava, R. A., Ed.; Academic Press: New York, 1980; Vol. 16, Part C, pp 315−377.
(47) Petropoulos, J. H. In *Polymeric Gas Separation Membranes*; Paul, D. R., Yampol'skii, Y. P., Eds.; CRC Press: Boca Raton, FL, 1994; pp 17−82.
(48) Bondar, V. I.; Freeman, B. D.; Yampolskii, Y. P. *Macromolecules* **1999**, *32*, 6163−6171.
(49) Reid, R. C.; Prausnitz, J. M.; Poling, B. E. *The Properties of Gases and Liquids*, 4th ed.; McGraw-Hill: New York, 1987.
(50) Wong, B.; Zhang, Z.; Handa, Y. P. *J. Polym. Sci., Part B: Polym. Phys.* **1998**, *36*, 2025−2032.
(51) Rodgers, P. A. *J. Appl. Polym. Sci.* **1993**, *48*, 1061−1080.
(52) Pottiger, M. T.; Laurence, R. L. *J. Polym. Sci., Polym. Phys. Ed.* **1984**, *22*, 903−907.
(53) Hariharan, R.; Freeman, B. D.; Carbonell, R. G.; Sarti, G. C. *J. Appl. Polym. Sci.* **1993**, *50*, 1781−1795.
(54) Daubert, T. E.; Danner, R. P. *Physical and Thermodynamic Properties of Pure Chemicals*; Hemisphere Publishers: New York, 1989.
(55) Sanchez, I. C.; Panayiotou, C. In *Models for Thermodynamic and Phase Equilibria Calculations*; Sandler, S. I., Ed.; Marcel Dekker: New York, 1994.
(56) Staudt-Bickel, C.; Koros, W. J. *J. Membr. Sci.* **1999**, *155*, 145−154.
(57) Pinnau, I.; He, Z.; Da Costa, A. R.; Amo, K. D.; Daniels, R. US Patent 6,361,582 B1, 2002.
(58) Pinnau, I.; He, Z.; Da Costa, A. R.; Amo, K. D.; Daniels, R. US Patent 6,361,583 B1, 2002.
(59) Prabhakar, R.; Freeman, B. D.; Roman, I. *Macromolecules* **2004**, *37*, 7688−7697.
(60) Freeman, B. D.; Pinnau, I. In *Polymer Membranes for Gas and Vapor Separation*; Freeman, B. D., Pinnau, I., Eds.; American Chemical Society: Washington, DC, 1999; Vol. 733, pp 1−27.

MA050546B